Research on Chemical Intermediates (2024) 50:3435–3452
https://doi.org/10.1007/s11164-024-05298-2

Green synthesis, characterization and antimicrobial efficacy of silver nanoparticles from *Kappaphycus alvarezii* extract

Syafiqah Syazwani Jaffar[1] · Suryani Saallah[1] · Mailin Misson[1] · Shafiquzzaman Siddique[1] · Jumardi Roslan[2] · Wuled Lenggoro[3]

Received: 29 February 2024 / Accepted: 27 April 2024 / Published online: 23 May 2024

Abstract

Silver nanoparticles (AgNPs) synthesized via a green method offer numerous advantages compared to conventional chemical synthesis routes, primarily due to their lower cost, non-toxic nature, and enhanced antimicrobial properties. This study introduces a green method for synthesizing AgNPs with promising antimicrobial properties, using *Kappaphycus alvarezii* (*K. alvarezii*), a red seaweed, as the reducing and stabilizing agent. The hydrothermal method was employed, and optimal synthesis conditions were identified at 90 °C for 2 h. The resulting AgNPs were comprehensively characterized using an array of spectroscopic and microscopic techniques including UV–Visible (UV–Vis) spectroscopy, fourier-transform infrared spectroscopy, X-ray diffraction spectroscopy, energy-dispersive X-ray spectroscopy, field emission scanning electron microscopy, transmission electron microscope, and atomic force microscopy. The findings indicated that the functional groups inherent to the seaweed extract played a crucial role in both reducing and stabilizing the AgNPs. The synthesized AgNPs are confirmed based on the presence of the characteristic surface plasmon resonance band within the 380–460 nm range in the UV–Vis spectra. The AgNPs are predominantly composed of silver (82.38 wt%) and exhibit a face-centered cubic lattice based on the distinct diffraction peaks observed at 2θ values of 38.06°, 44.23°, 64.34°, and 77.27° align with the (1 1 1), (2 0 0), (2 2 0), and (3 1 1) reflection planes. Microscopic analysis revealed a cubical shape of the nanoparticles with rough surfaces consisting of spherical nanoparticles measuring 1–8 nm in diameter. The AgNPs displayed potent antimicrobial activity against a range of pathogens including *Escherichia coli* (*E. coli*), *Klebsiella pneumoniae* (*K. pneumoniae*), *Staphylococus aureus* (*S. aureus*), *Bacillus subtilis subsp. spizizenii* (*B. subtilis*), and *Candida albicans* (*C. albicans*) with minimum inhibitory concentrations and minimum bactericidal/fungicidal concentrations as low as 0.13 mg/mL. These findings highlight the potential of *K. alvarezii* as reducing agent for the production of AgNPs, which hold great promise as antimicrobial agents in various food and biomedical applications.

Extended author information available on the last page of the article

Keywords Seaweed · Stabilizing agent · Hydrothermal · Antimicrobial resistance

Introduction

The advent of nanobiotechnology, an interdisciplinary field merging nanotechnology and biotechnology has revolutionized myriad sectors, promising substantial advancements in diverse fields ranging from medicine such as to environmental science. One of the most significant breakthroughs in the nanobiotechnology domain is the emergence of environmentally friendly synthesis routes for nanoparticles (NPs) including AgNPs, renowned for their unique physicochemical properties, including high thermal and electrical conductivity, chemical stability, and potent antimicrobial efficacy [1, 2]. AgNPs find wide-ranging applications in fields such as targeted drug delivery for cancer therapy, wound healing, antimicrobial agents, biosensing for disease diagnosis, tissue engineering for regenerative medicine, and environmental remediation for water purification and air filtration [3–5].

Traditionally, the production of AgNPs has been dominated by chemical synthesis methods. However, these techniques often involve the use of toxic chemicals, which pose environmental and health risks, thus stirring interest in more eco-friendly alternatives [6]. Given the present environmental concerns and the possibility of AgNPs cytotoxicity once released into the environment, the emergence of the 'green synthesis' approach, a sustainable method that leverages biological entities including plant extracts [7], fungi [8], and bacteria [9] was used to synthesize these nanoparticles. The phytoconstituents in these biomolecules such as glycosides, terpenoids, alkaloids, and phenolics are mostly found in charge of reducing silver ions into AgNPs [3].

Among the various biological entities, seaweeds have recently garnered attention as a potential resource for the green synthesis of AgNPs [10]. Various species of seaweed such as *Ulva lactuca* [11], *Sargassum polycystum* [2], *Galaxaura rugosa* [12], *Turbinaria ornata* [13] and *Pulicaria vulgaris* [14] have been studied for this purpose due to their high metal uptake capacity and accessibility, which is a distinct advantage amongst the other bioreducing agents [12]. Furthermore, seaweeds are abundance in nature and rich source of polysaccharides, phytochemicals and secondary metabolites that can reduce silver ions into AgNPs [15].

In this context, *Kappaphycus alvarezii* seaweed has been identified for its potential in the green synthesis of AgNPs. *Kappaphycus alvarezii* is an important industrial red alga known for its high carrageenan content, a linear water-soluble sulphated polysaccharide widely utilized as a gelling agent in the food and pharmaceutical industries [15]. This seaweed species is extensively cultivated in coastal waters across the Southeast Asia region, including Malaysia, Indonesia, and the Philippines [16] owing to its rapid growth rate, capable of doubling in approximately 15–30 days [17, 18]. Besides being an important source of polysaccharides, *K. alvarezii* is highly sought after due to the presence of biologically active compounds such as phenolic lipids, terpenoid derivatives, and phlorotannins. These compounds are associated with antimicrobial properties and offer various benefits in numerous application [15, 19].

Existing literature provides initial insights into the synthesis of AgNPs using *K. alvarezii*, with methods such as aqueous extract reduction being commonly utilized [15, 19, 20]. Despite the promising findings, the potential of *K. alvarezii* in the hydrothermal synthesis of AgNPs and its subsequent antimicrobial effects against a broad range of microorganisms has not yet been explored. This represents a significant knowledge gap, as the hydrothermal method can enhance the control over size and distribution of nanoparticles, and the antimicrobial properties of AgNPs are of particular interest in the current era of increasing antibiotic resistance.

In this study, the effect of hydrothermal reaction conditions on the green synthesis of AgNPs using *K. alvarezii* and the antimicrobial properties of the synthesized AgNPs against broad-spectrum microorganisms including Gram-negative and Gram-positive bacteria as well as fungi were investigated for the first time. Findings from this study may stimulate the development of sustainable nanotechnology practices for AgNPs synthesis, aligning with global efforts toward environmental sustainability and may potentially contribute to various industrial applications of AgNPs including healthcare, water treatment, and food packaging.

Experimental section

Materials and microorganisms

K.alvarezii seaweed (Fig. 1) was purchased from a local supplier in Semporna, Sabah, Malaysia. Silver nitrate ($AgNO_3$, 99.7%) was obtained from Systerm (Classic Chemicals Sdn. Bhd., Shah Alam, Malaysia). Luria Bertani (LB) agar and broth (MILLER), Mueller Hinton Agar (MHA) and Mueller Hinton Broth (MHB) used in antimicrobial studies were supplied by Merck & Co (Darmstadt, Germany). The

Fig. 1 *Kappaphycus alvarezii* seaweed collected from Semporna, Sabah, Malaysia

microorganisms' strains, *Escherichia coli* (ATCC 25922), *Klebsiella pneumoniae* (ATCC 700603), *Staphylococus aureus* (NCTC 12493), *Bacillus subtilis subsp. spizizenii* (ATCC 6633), and *Candida albicans* (ATCC 60193) were obtained from KWIK-STIK™ (Microbiologics Inc., Minnesota, USA). Millipore deionised water was used throughout this work.

Preparation of aqueous seaweed extract

1 g of washed dried *K. alvarezii* was weighed and soaked overnight in 100 mL of distilled water. The mixture was stirred at 60 °C for 15 min then filtered using double cheesecloth and Whatman filter paper. The filtrate was kept in the refrigerator for further usage [15].

Synthesis of AgNPs

Aqueous seaweed extract was mixed with $AgNO_3$ (0.1 M) solution in a ratio of 1:3 (v/v). The mixture was subjected to hydrothermal reaction using hotplate stirrer under constant stirring (400 rpm) with varying temperature (50–100 °C) and reaction time (1–4 h). The experimental conditions were chosen based on previous similar studies [21–23] which highlighted the effect of low-to-high temperature and reaction time. The change in the color of the solution was monitored as an indicator of AgNPs formation. Upon completion of the reaction, the solution was allowed to cool to room temperature prior to centrifugation at 7500 rpm (25 °C) for 15 min. The supernatant was subsequently discarded, and the residual solvent was eliminated through washing using ethanol. The final product underwent an evaporative drying at room temperature to yield solid AgNPs [24]. A schematic representation illustrating the green synthesis of AgNPs utilizing seaweed extract, along with the general mechanism is depicted in Fig. 2.

Characterization of AgNPs from *K. alvarezii*

UV–Vis spectroscopy

Agilent Cary 60 UV–Vis spectrometer was used to record the absorbance spectra of the AgNPs in the wavelength range of 300–500 nm. The absorbance was recorded in a quartz cuvette with a 1-cm path length. For the baseline correction, distilled water was used as a blank.

FTIR spectroscopy

FTIR analysis was performed using an Agilent Cary 630 FTIR spectrometer (Agilent Technologies Inc., USA) to identify the functional groups present in the sample and to examine the chemical interaction between the seaweed extract and the AgNPs. Spectra were collected at 25 °C within the infrared range of 600–4000 cm^{-1} with a spectral resolution of 4 cm^{-1} and 32 scans.

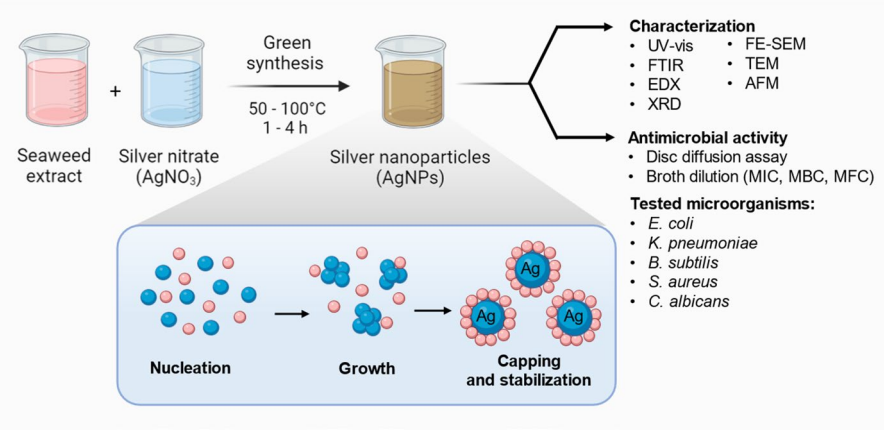

Fig. 2 Schematic representation of the green synthesis process for AgNPs utilizing the extract from *K. alvarezii* seaweed, along with an overview of the general mechanism involved (Adapted from [25]). The image was partly created with BioRender.com

XRD spectroscopy

Using an X-ray diffractometer (Rigaku SmartLab, Rigaku Corporation, Tokyo, Japan) set to 40 kV and 50 mA, the crystallographic data of the AgNPs was acquired. A Cu-Kα radiation source with a wavelength of 1.54 Å was used to scan the AgNPs over the diffraction angle (2θ) range of 3°–80°. At a temperature of 25 °C, the analysis was conducted continuously at a scan speed of 4.00°/min.

EDX spectroscopy

EDX spectroscopy was employed for elemental analysis using Bruker Nano GmbH instrument (Berlin, Germany). The primary energy level for the analysis was set at 15 keV. The instrumentation was equipped with an XFlash 5010 detector to facilitate the detection and quantification of the elemental composition within the samples.

FE-SEM analysis

Morphological information regarding the surface characteristics of AgNPs was obtained using FE-SEM instrument (JEOL JSM7900F, Tokyo, Japan). To facilitate the observation, the sample was securely mounted on a stub using double-sided black conducting tape. The FE-SEM analysis was performed under vacuum conditions at an accelerating voltage of 5 kV.

TEM analysis

The shape and size of the AgNPs were determined using a Tecnai G2 Spirit BioTWIN TEM system (FEI, USA) operating at a voltage of 80 kV. Before analysis, the AgNPs suspension was diluted and subjected to 1-h ultrasonic treatment in an Ultrasonic Bath Sonicator. A droplet of the resultant suspension was deposited onto TEDPELLA Support Films (Formvar/Carbon 300 mesh, Copper, 63 µm grid hole size). The sample was subsequently dried for 20 min at 60 °C to secure the AgNPs onto the support film. The particle size and size distribution were determined by processing the captured TEM images using ImageJ analysis software (NIH, USA). A minimum of 120 particles were measured to ensure the statistical significance of the results.

AFM analysis

Topographical imaging was conducted using a Dimension Icon AFM instrument (Bruker, Santa Barbara, CA, USA) with a scanning speed of 0.6 line/s. Prior to the analysis, a drop of the diluted AgNPs suspension was spread on a glass substrate and left to dry at room temperature after being pulse-sonicated for 5 min.

Antimicrobial activity of AgNPs-seaweed

Disc diffusion assay

The antimicrobial efficacy of the synthesized AgNPs was assessed using the agar disc diffusion method [26]. Two representative Gram-positive bacteria, *S. aureus* and *B. subtilis*, two representative Gram-negative bacteria, *E. coli* and *K. pneumoniae*, and the fungal species *C. albicans* were chosen as test microorganisms. Microbial cells from glycerol stocks were streaked on agar plates and incubated overnight at 37 °C to obtain individual colonies. These colonies were then inoculated in LB broth and incubated overnight at 37 °C to cultivate the bacterial cultures for the antimicrobial study. The disc diffusion assay was performed on MHA plates that were initially inoculated with bacterial and fungal solutions spread evenly using a sterile swab. Subsequently, sterile blank discs measuring 5.5 mm in diameter were loaded with 0.05 mg/ml ampicillin (positive control), sterile water (negative control), seaweed extract and the synthesised AgNPs (0.05 mg/ml). The discs were then allowed to air dry before being placed onto the agar plates. The plates were incubated overnight at 37 °C and the resulting zones of inhibition formed on the agar were measured for each plate. To investigate the effect of AgNPs concentration on antimicrobial activity, the same procedures were repeated using different concentrations of AgNPs ranging from 0.1 to 1 mg/mL. The antimicrobial assay was performed in triplicate.

Broth dilution assay

The inhibitory effect of the AgNPs against the test microorganisms (*S. aureus*, *B. spizizenii*, *E. coli*, *K. pneumoniae,* and *C. albicans*) was assessed using the standard broth dilution method. A twofold dilution series was prepared to obtain different concentrations of AgNPs ranging from 0.002 to 1 mg/mL. Fresh single colonies of the microorganism cultures were inoculated in MHB medium and incubated for 18 h at 37 °C. The resulting cultures were then mixed with AgNPs solutions of varying concentrations and incubated at 37 °C for another 18 h. Post-incubation, the optical density of the cultures at 600 nm (OD_{600}) was measured using a microplate reader (Tecan's Sunrise). The minimum concentration of AgNPs that completely inhibited the growth of the microorganisms was determined as the Minimum Inhibitory Concentration (MIC). To determine the Minimum Bactericidal Concentration (MBC) and Minimum Fungicidal Concentration (MFC), the cultures were streaked on MHA plates and incubated for 18 h at 37 °C. MBC and MFC were defined as the lowest concentration of AgNPs that resulted in no visible growth of bacteria and fungi on the agar plates, respectively. All experiments were performed in triplicate [27].

Results and discussion

Green synthesis of AgNPs

In the present investigation, hydrothermal reaction was employed for the green synthesis of AgNPs, utilizing $AgNO_3$ as the precursor and seaweed extract as both reducing and stabilizing agents. The effect of temperature (50–100 °C) and reaction time (1–4 h) on the AgNPs synthesis were investigated, as these parameters are known to influence the kinetics of nucleation and growth, ultimately affecting the size and stability of the nanoparticles. The progression of the reaction was monitored by observing the changes in color of the reaction mixture, which is indicative of nanoparticle formation due to the surface plasmon resonance (SPR) phenomenon and was further confirmed using absorbance spectra recorded by UV–VIS spectrometer.

Effect of temperature

Figure 3a, b depicts the results of silver AgNPs synthesised at different temperatures. As the temperature increased, the initially colorless solution gradually turned into a brownish hue, indicating the progress of AgNPs formation. The UV–Vis spectra revealed a gradual enhancement in the intensity of the absorption band in the 380–460 nm as the temperature was raised from 50 to 80 °C. A substantial and distinct peak in intensity was observed at 90 °C, which indicated the formation and growth of AgNPs with narrow size distribution. The underlying mechanism for this phenomenon can be elucidated by the accelerated kinetics of the reduction process at elevated temperatures [28]. Specifically, the enhanced thermal energy at higher temperatures facilitates more rapid reduction of Ag^+ by the active phytochemical

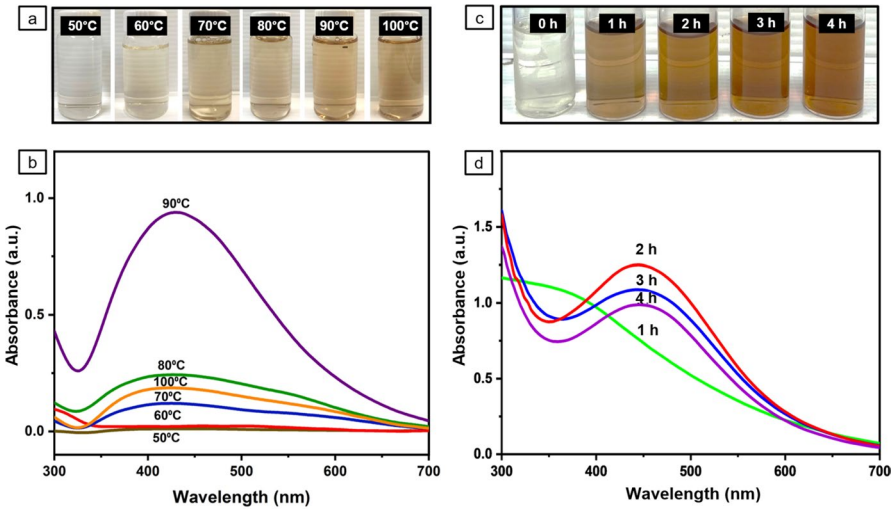

Fig. 3 Visual observation and UV–Vis spectrum of AgNPs produced with varying temperature of 50–100 °C (**a**, **b**) and reaction time (**c**, **d**)

components present in the seaweed extract. Consequently, this leads to an improved production rate of AgNPs and their subsequent growth.

However, when the reaction temperature reached 100 °C, the absorption peak corresponding to the SPR band exhibited a significant reduction. The decline in UV–vis absorbance at this high temperature can be attributed to several factors, including nanoparticle aggregation, changes in size and shape, a decrease in effective nanoparticle concentration, and possible surface modifications, as reported in previous studies [29, 30]. Based on these findings, a reaction temperature of 90 °C offers the optimal condition for the formation of AgNPs.

Effect of reaction time

A sufficient reaction time plays a pivotal role in achieving optimal nucleation and subsequent nanoparticle stabilization. Figure 3c, d shows the color transformations and the UV–Vis absorption spectra and observed during the reduction process over various incubation periods. The reaction mixture initially appeared colorless, but as the reaction progressed, it gradually transitioned to a brownish hue. The UV–Vis spectrum of the reaction mixture incubated for 1 h displayed an absence of the characteristic SPR band within the 380–460 nm range. However, as the reaction time extended to 2 h, a significant increase in absorbance was observed, indicating active conversion of silver ions to AgNPs, leading to an increase in nanoparticle concentration [31]. Subsequently, when the reaction time was further extended to 3 and 4 h, a decrease in absorbance was noted. Despite the noticeable changes in the reaction mixture's deeper brownish hue after two hours suggesting that more particles were formed, the spectra data indicated that aggregation was most likely to begin. This trend suggests that the reduction and stabilization of AgNPs reached equilibrium at

2 h. Similar to the effect observed with temperature, a longer reaction time did not result in a significant increase in the SPR associated with AgNPs formation. It is likely that most of the silver ions may have already been converted into nanoparticles and further extension of the reaction time would lead to adverse effects, including aggregation which alters the optical properties of the AgNPs [1, 32].

Characterizations of AgNPs

FTIR analysis

The FTIR spectroscopy analysis revealed important information regarding the chemical functionality and interaction between the seaweed extract and the AgNPs. As depicted in Fig. 4a, the seaweed extract demonstrated a wide absorption band in the 3200–3600 cm^{-1} region attributed to O–H stretching vibrations [33]. The peak at 2865 cm^{-1} denotes C-H stretching vibrations related to aliphatic hydrocarbons or methyl groups. A distinct peak at 1646 cm^{-1} is indicative of the

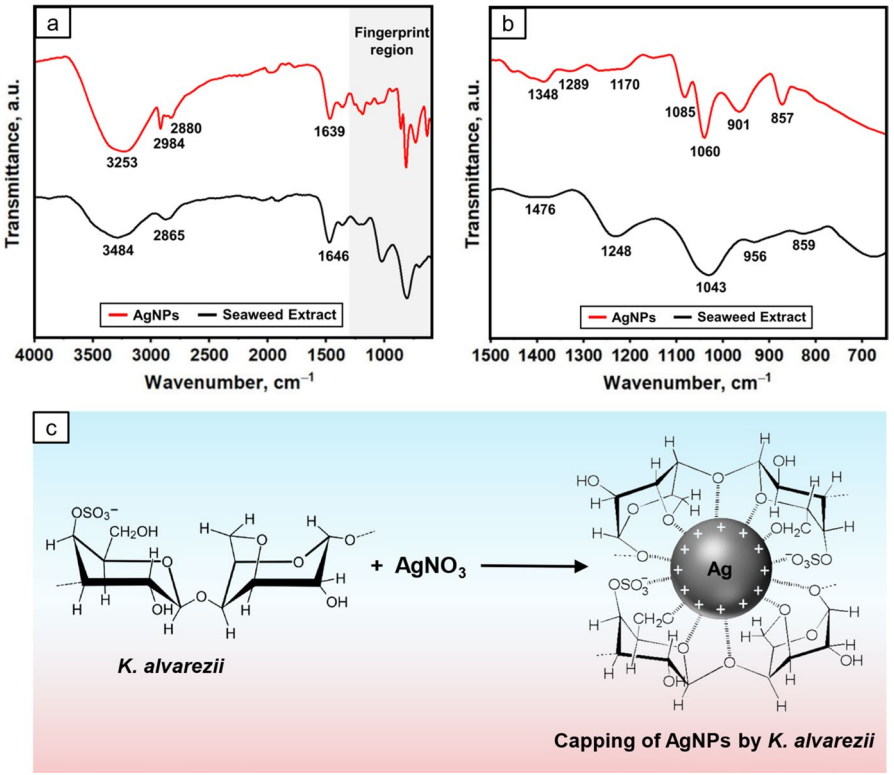

Fig. 4 FTIR spectra of seaweed extract and AgNPs (**a**); the corresponding fingerprint region (**b**); and **c** Mechanism of capping of AgNPs by functional groups present in the *K. alvarezii* seaweed extract. *Source*: Adapted from [36]

C=O asymmetric stretching of carbonyl groups [34]. In the fingerprint region of the seaweed extract shown in Fig. 4b, peaks at 1476 cm^{-1} and 1248 cm^{-1} correspond to the stretching vibration of sulfate groups [19]. The peak at 1043 cm^{-1} is linked to the C–O stretching band of the C–O–SO_3 group while peaks at 956 cm^{-1} and 859 cm^{-1} are attributed to 3,6-anhydro-D-galactose and galactose-4-sulfate, respectively [35], consistent with the sulphate content commonly found in red seaweed. Comparatively, the AgNPs display a narrower absorption band in the 3200–3400 cm^{-1} range, and a peak shift to a lower wavenumber suggesting the involvement of O–H groups from the seaweed in the nanoparticle synthesis [13]. The peak shift from 1646 to 1639 cm^{-1} and the absence of the 1248 cm^{-1} peak in the AgNPs' spectrum implies the involvement of carbonyl and sulphate ester groups in the formation of the AgNPs [1]. Strong absorption bands in the 1000–1100 cm^{-1} region validate the conjugation of the C–O–SO_3 group from the seaweed extract to the AgNPs surface [5]. These findings collectively demonstrate the role of functional groups present in the seaweed extract in the reduction and stabilization of the AgNPs as illustrated in Fig. 4c [36], aligning with previous studies [13, 19, 24].

Energy-dispersive X-ray (EDX) analysis

The EDX pattern in Fig. 5 provides insight into the elemental composition of the sample. Metallic silver typically presents a distinct optical absorption peak at 3 keV, a phenomenon associated with SPR [37, 38]. A prominent signal at 3 keV corresponding to silver (Ag) and the high elemental silver composition (82.38%) confirm the successful formation of AgNPs. Other elements such as carbon (C), oxygen (O), and chlorine (Cl) is likely originated from organic compounds from the seaweed extract adhering to the surface of the AgNPs [31]. This interaction between the organic compounds and the AgNPs may play a role in stabilizing the nanoparticles.

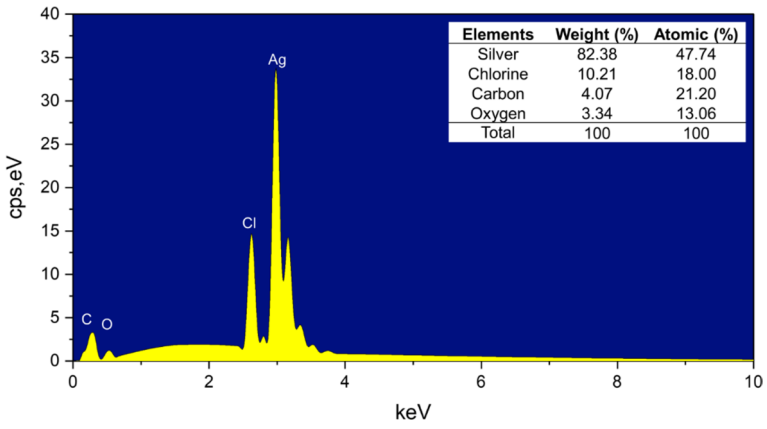

Fig. 5 EDX Spectra of AgNPs and the corresponding elemental composition

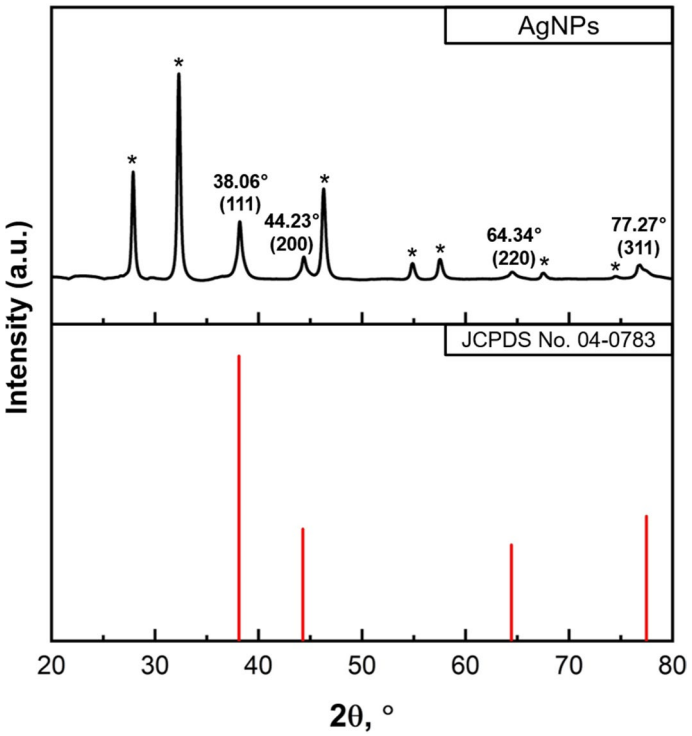

Fig. 6 XRD pattern of the AgNPs and silver (JCPDS No. 04-0783)

X-ray diffraction (XRD) analysis

Figure 6 presents the XRD spectra of the AgNPs, affirming their crystalline nature. Four distinct diffraction peaks observed at 2θ values of 38.06°, 44.23°, 64.34° and 77.27° align with the (1 1 1), (2 0 0), (2 2 0), and (3 1 1) reflection planes of the face-centered cubic (fcc) structure of silver as per the database of Joint Committee on Powder Diffraction Standards (JCPDS card number 04-0783) [31]. In addition to these Bragg peaks that are indicative of silver nanocrystals, additional peaks marked with an asterisk (*) were also detected at 27.88°, 32.28°, 46.27°, 54.93°, 57.50°, 67.47° and 74.55°. The presence of these peaks can be ascribed to the seaweed extract which contains organic compounds responsible in reducing silver ions and stabilizing the resultant nanoparticles [39], in agreement with the FTIR and EDX data. Similar findings have also been reported for the AgNPs synthesised using plant extracts such as those from *Tectona grandis* seeds [38], banana peel [39], *Allium ampeloprasum* extract [40] and *Lysiloma acapulcensis* [6].

Structural properties and morphology of AgNPs

The FESEM image in Fig. 7a reveals distinct cubical-shaped AgNPs. These particles exhibit rough-textured surfaces, with the cubic units averaging 50 nm in

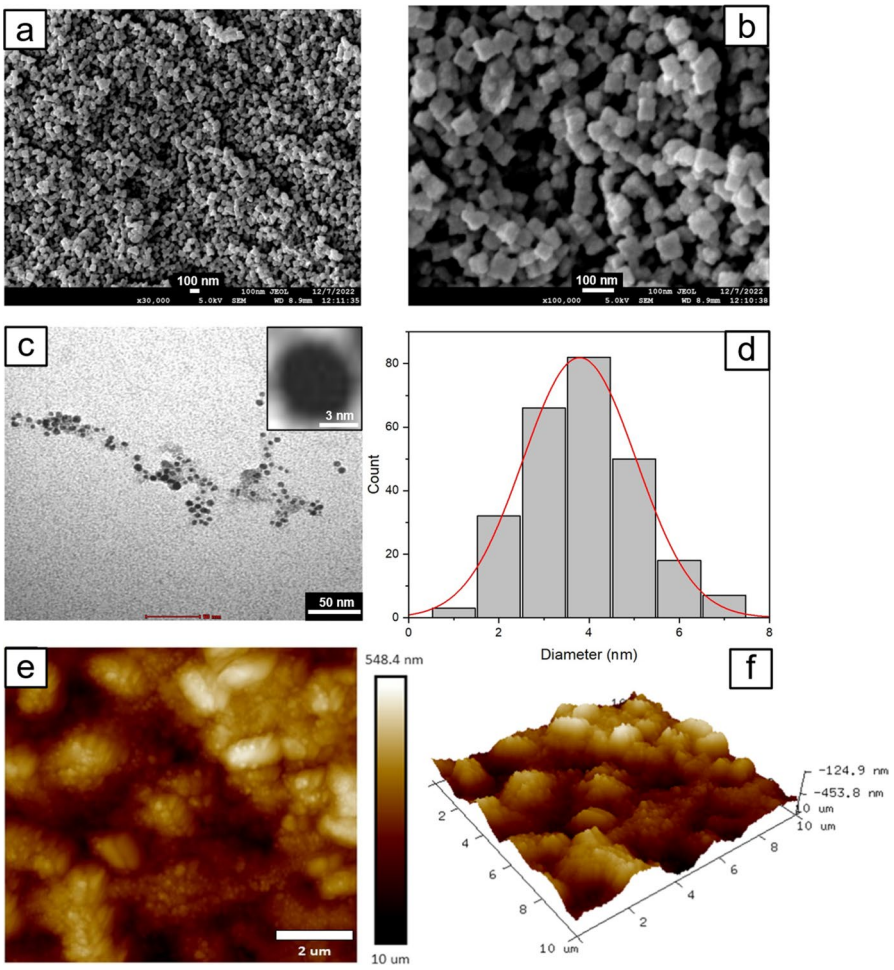

Fig. 7 Morphological analysis of the AgNPs. **a**, **b** FE-SEM image and the corresponding particle size distribution; **c**, **d** TEM images and the corresponding particle size distribution

diameter. A closer examination suggests that these cubic formations are clusters of smaller spherical nanoparticles (Fig. 7b). This is corroborated by TEM analysis which confirms the presence of uniformly distributed spherical AgNPs within the seaweed matrix, with diameters ranging from 1 to 8 nm (Fig. 7c, d). It is noteworthy that the AgNPs in the TEM image is well separated without aggregation. The aggregation of AgNPs into cubic structures as observed in the FESEM image is likely a result of the self-assembly process induced by the drying effect with ethanol. This phenomenon was observed by Sun et al. [41] in a study involving the addition of ethanol to cetyltrimethylammonium bromide (CTAB) capped AgNPs. The exposure to ethanol resulted in the partial removal of the protective layer derived from seaweed extract that bound to the AgNPs, thereby promoting aggregation. Similar

aggregation behaviour was also reported by Hemlata et al. [42] for AgNPs synthesised using *Cucumis prophetarum* aqueous leaf extract. These findings suggest that the protective bioorganic compounds from the seaweed extract not only facilitate the reduction of silver ions but also influence the aggregation behavior of the nanoparticles in the dry state.

The AgNPs' spherical with rough-textured surfaces is further confirmed by the topographical AFM scanning of the sample in Fig. 7e similar to other findings [43, 44]. The 3D structure in Fig. 7f shows the height analysis of the surface of AgNPs which the roughness of the sample can be estimated based on *Rq* and *Ra* value. From the result analysis, the AgNPs sample shows a high surface roughness as the *Rq* value of the sample is 72.1 nm which represents the square root of the sum of individual heights and depths from the mean line, and *Ra* value of 58.1 nm which denotes by arithmetic average of surface heights measured over a surface. The high surface roughness is particularly useful in the context of antimicrobial application as rough surfaces can increase the surface area of the nanoparticles, thus providing more contact area with microorganisms, improving their effectiveness in inhibiting microbial growth [45].

The formation of AgNP was confirmed by the existence of diffraction patterns of silver crystal structure, matching with the standard X-ray diffraction (XRD) pattern (JCPDS no. 04-0783). The diffraction peaks for both samples at 38.1°, 44.3°, 64.5°, and 77.4° represent the crystallographic planes of (111), (200), (220), and (311) for the face-centered cubic of the silver crystal. These have further confirmed the formation of Ag crystals in both samples by using microwave irradiation method.

Antimicrobial activity of AgNPs

Disk diffusion assay

The antimicrobial activity of the AgNPs was assessed using the disk diffusion assay, employing Gram negative bacteria (*E. coli* and *K. pnuemoniae*), Gram-positive bacteria (*S. aureus* and *B. subtilis*) and fungal species *C. albicans* as the test microorganisms. Examination of the agar plates presented in Fig. 8 reveals that all the tested microorganisms display susceptibility to AgNPs, as evidenced by distinct zones of inhibition surrounding the agar disks. These zones of inhibition signify the ability of AgNPs to impede the growth of the tested microorganisms thus affirming their potent antimicrobial properties. The antimicrobial action of AgNPs involves several mechanisms including oxidative stress, intracellular adhesion, penetration, and disruption of organelles and biomolecules [38, 46, 47]. Notably, the electrostatic properties of AgNPs play a crucial role in their interaction, enabling them to traverse the bacterial cell membrane and causing changes in membrane permeability and molecular composition. A number of studies [48, 49] indicates that electrostatic interactions occur between carboxyl, phosphate, and amino groups within the bacterial cell wall and the positively charged silver ions. This interaction leads to the adhesion of AgNPs to the microorganism's cell wall, establishing a complex interplay between AgNPs and bacterial structures.

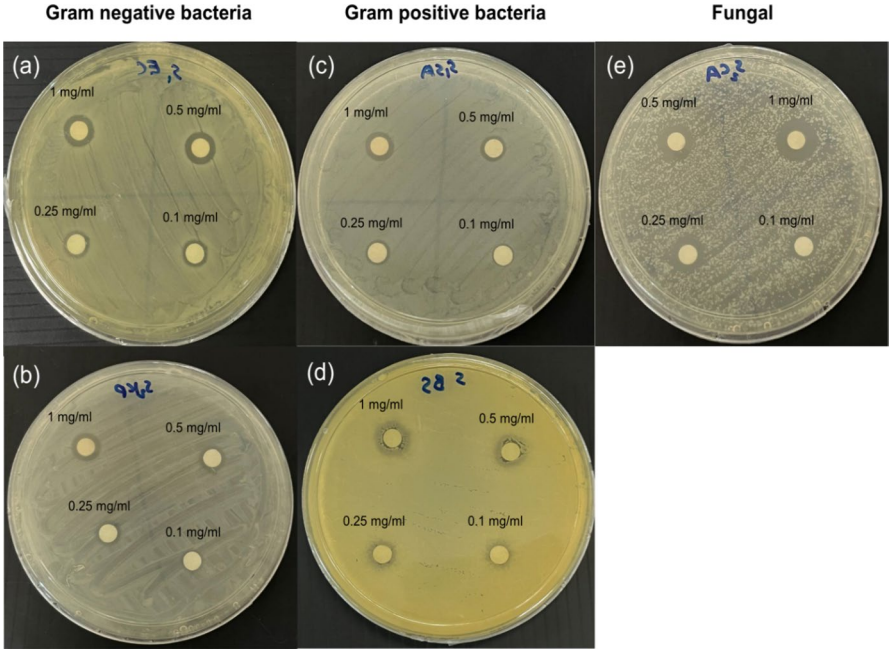

Fig. 8 Representative agar plates of the disk diffusion assay of AgNPs with the concentration of 0.1–1 mg/mL against selected Gram-negative bacteria **a** *E. coli* and **b** *K. pneumoniae*; Gram-positive bacteria **c** *S. aureus* and **d** *B. subtilis*, and fungal pathogen **e** *C. albicans*

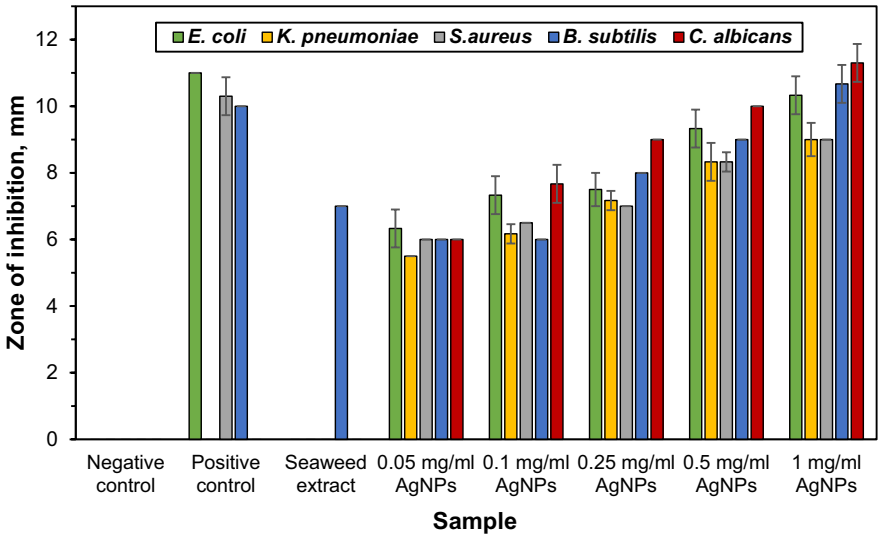

Fig. 9 Zone of inhibition expressed in mm measured from disk diffusion assay

The concentration-dependent antimicrobial activity of AgNPs is evident based on the zone of inhibition in Fig. 9, with higher concentrations correlating with increased efficacy. Notably, *B. subtilis* and *E. coli* exhibit greater susceptibility to AgNPs compared to *K. pneumoniae* and *S. aureus*. The variability in susceptibility observed can be explained by considering the diverse structural and physiological attributes inherent in the tested bacterial strains [50]. The finding also shows that *K. pneumoniae* is resistant to ampicillin (positive control) but displays susceptibility to AgNPs, affirming the broad-spectrum antibacterial efficacy of AgNPs, particularly against multidrug-resistant bacterial strains [12]. Of particular interest is the notable fungicidal activity of AgNPs against *C. albicans*, as shown by the larger zone of inhibition compared to bacterial species. This observation aligns with findings by Garibo et al. (2020) who reported similar results for AgNPs synthesized using *Lysiloma acapulcensis* [6].

Minimum inhibitory concentration (MIC), minimum bactericidal concentration (MBC) and minimum fungicidal concentration (MFC) of AgNPs

The Minimum Inhibitory Concentration (MIC), Minimum Bactericidal Concentration (MBC), and Minimum Fungicidal Concentration (MFC) represent critical parameters that define the efficacy of antimicrobial agents. The MIC is the minimum concentration of an antimicrobial necessary to inhibit microbial proliferation, whereas MBC and MFC refer to the minimum concentrations that are lethal to bacteria and fungi, respectively [13].

As shown in Table 1, the MIC was consistently observed at 0.13 mg/ml for all tested microorganisms. This concentration is the threshold at which AgNPs demonstrate significant inhibition of microbial growth. The consistency of MIC

Table 1 MIC, MBC, and MFC values of AgNPs synthesized using various seaweed species

Seaweed species	Tested strain	MIC	MBC/MFC	References
Galaxaura rugosa	*E. coli*	0.75	1.125	[12]
	K. pneumoniae	9.00	> 18	
	S. aureus	1.125	2.25	
Turbinaria ornata	*E. coli*	0.125	0.25	[13]
	K. pneumoniae	0.25	0.5	
	S. aureus	0.0625	0.125	
Ulva lactuca	*E. coli*	0.062–0.5	0.125–0.5	[11]
	K. pneumoniae	0.5	0.5	
	S. aureus	0.25	0.25	
Kappaphycus alvarezii	*E. coli*	0.025–0.05	0.05–0.10	[15]
Kappaphycus alvarezii	*E. coli*	0.13	0.25	Present study
	K. pneumoniae	0.13	0.25	
	S. aureus	0.13	0.13	
	B. subtilis	0.13	0.13	
	C. albicans	0.13	0.25	

values across different strains highlights the broad-spectrum and potent antimicrobial action of AgNPs. In terms of MBC, both *S. aureus* and *B. subtilis* showed MBC values equal to their MIC at 0.13 mg/ml suggests that the AgNPs synthesized through green methods are not only inhibitory but also bactericidal at this concentration. Conversely, a higher concentration of 0.25 mg/ml was necessary to reach MBC for *E. coli* and *K. pneumoniae* and MFC for *C. albicans*, indicating a need for an increased concentration of AgNPs to exert a lethal effect on these organisms. The AgNPs produced in the current study are more effective than those derived from *G. rugosa* [12], as indicated by lower MIC and MBC values and have similar effectiveness to AgNPs derived from *T. ornata* [13] and *U. lactuca* [11]. The study by Khan et al. [15] on AgNPs synthesized using *K. alvarezii* extract showed promising MIC and MBC values but was limited to testing against *E. coli*. The observed variability in MIC, MBC, and MFC values across these studies suggests that the antimicrobial potency of AgNPs is influenced by multiple factors, including the method of nanoparticle synthesis, the intrinsic properties of the seaweed species used, and the physiological characteristics of the target microorganisms.

Conclusions

The current study has effectively demonstrated that hydrothermal synthesis utilizing *K. alvarezii* aqueous extract is a viable and eco-friendly approach for producing AgNPs. Appropriate selection of synthesis conditions, particularly at 90 °C for 2 h, facilitated the production of AgNPs with desirable characteristics in terms of size, shape, crystal structure and antimicrobial potency. The synthesis of AgNPs involves a straightforward experimental procedure with minimal use of chemicals, supporting the adoption of green synthesis approach. The instrumental analyses including UV–Visible spectroscopy, FTIR, XRD, EDX, FE-SEM, TEM, and AFM collectively confirmed the successful reduction and stabilization of AgNPs, highlighting the significant role of biomolecules in the seaweed extract. The comprehensive antimicrobial assays provided compelling evidence of the AgNPs' potent efficacy against a spectrum of pathogens including Gram-positive bacteria, Gram-negative bacteria, and fungi, showcasing their potential as an effective agent in combating microbial resistance. These findings provide a promising avenue for the application of the synthesized AgNPs, particularly in food preservation and biomedical products.

Acknowledgements This work was supported by Universiti Malaysia Sabah (UMSGreat Grant No. GUG0550).

Author contributions S.S. (Suryani Saallah), W.L., J.R., S.S. (Shafiquzzaman Siddiquee), M.M. contributed to conceptualization; S.S.J. done investigation; S.S.J. helped in writing—original draft preparation; S.S. (Suryani Saallah), J.R., and S.S.J. done writing—review and editing; S.S. (Suryani Saallah) and S.S.J. helped in funding acquisition; S.S. (Suryani Saallah), S.S. (Shafiquzzaman Siddiquee), and M.M. done supervision

Data availability No datasets were generated or analysed during the current study.

Declarations

Conflict of interest The authors declare no conflict of interest.

References

1. H. Wan, C. Li, S. Mahmud, H. Liu, Colloids Surf. A Physicochem. Eng. Asp. **616**, 126325 (2021)
2. R. Thiurunavukkarau, S. Shanmugam, K. Subramanian, P. Pandi, G. Muralitharan, M. Arokiarajan, K. Kasinathan, A. Sivaraj, R. Kalyanasundaram, S.Y. AlOmar, V. Shanmugam, Sci. Rep. **12**, 14757 (2022)
3. N. Tarannum, D. Divya, Y.K. Gautam, RSC Adv. **9**, 34926 (2019)
4. R. Algotiml, A. Gab-Alla, R. Seoudi, H.H. Abulreesh, M.Z. El-Readi, K. Elbanna, Sci. Rep. **12**, 2421 (2022)
5. S. Pandey, J.Y. Do, J. Kim, M. Kang, Carbohydr. Polym. **230**, 115597 (2020)
6. D. Garibo, H.A. Borbón-Nuñez, J.N.D. de León, E. García Mendoza, I. Estrada, Y. Toledano-Magaña, H. Tiznado, M. Ovalle-Marroquin, A.G. Soto-Ramos, A. Blanco, J.A. Rodríguez, O.A. Romo, L.A. Chávez-Almazán, A. Susarrey-Arce, Sci. Rep. **10**, 12805 (2020)
7. C. Vanlalveni, S. Lallianrawna, A. Biswas, M. Selvaraj, B. Changmai, S.L. Rokhum, RSC Adv. **11**, 2804 (2021)
8. M.E. Beltrán Pineda, L.M. Lizarazo Forero, yC.A. Sierra, BioMetals **36**, 745 (2023)
9. T. Mustapha, N. Misni, N.R. Ithnin, A.M. Daskum, N.Z. Unyah, Int. J. Environ. Res. Public Health **19**, 674 (2022)
10. R. Chaudhary, K. Nawaz, A.K. Khan, C. Hano, B.H. Abbasi, S. Anjum, Biomolecules **10**, 1 (2020)
11. A.R. Hamouda, A.M. Alharthi, S.A. Alotaibi, M.A. Alenzi, A.D. Albalawi, Molecules **28**, 6324 (2023)
12. R.R. Alzahrani, M.M. Alkhulaifi, N.M. Alenazi, N.M. Almusayeib, M. Amina, M.A. Awad, A.H. Elmubarak, N.S. Aldosari, J. Taibah Univ. SCI **14**, 1651 (2020)
13. C.T.D. Raj, K. Muthukumar, H.U. Dahms, R.A. James, S. Kandaswamy, Front. Microbiol. **14**, 1 (2023)
14. M. Sharifi-Rad, P. Pohl, Nanomaterials **10**, 1 (2020)
15. M.S. Khan, S. Ranjani, S. Hemalatha, Mater. Chem. Phys. **282**, 125985 (2022)
16. C. Santhanaraju Vairappan, *Advances in Probiotics* (Elsevier, Amsterdam, 2021), p.247
17. R.S. Jalal, K.J. Jalani, I.A. Wahab, Z. Eshak, A.H. Ibrahim, H.F. Mohsin, J. Sustain. Sci. Manag. **18**, 187 (2023)
18. S.M. Mohammad, M. Razali, M. Rozaiman, N.H.N. Laizani, N. Zawawi, IFRJ **26**, 1677 (2019)
19. M. Faried, K. Shameli, M. Miyake, A. Hajalilou, K. Kalantari, Z. Zakaria, H. Hara, N.B.A. Khairudin, Res. Chem. Intermed. **42**, 7991 (2016)
20. P.C. Silva, V. Ganesan, J. Aruna Devi, A. Astalakshmi, P. Nima, A. Thangaraja, IJEAT **2**, 559 (2013)
21. A. Mohammed Fayaz, K. Balaji, P.T. Kalaichelvan, R. Venkatesan, Colloids Surf. B Biointerfaces **74**, 123 (2009)
22. A. Elgamouz, H. Idriss, C. Nassab, A. Bihi, K. Bajou, K. Hasan, M.A. Haija, S.P. Patole, Nanomaterials **10**, 1 (2020)
23. M.F. Zayed, R.A. Mahfoze, S.M. El-kousy, E.A. Al-Ashkar, Colloids Surf. A Physicochem. Eng. Asp. **585**, 124167 (2020)
24. S.S. Jaffar, S. Saallah, M. Misson, S. Siddiquee, J. Roslan, W. Lenggoro, Molecules **28**, 907 (2023)
25. B. Uzair, A. Liaqat, H. Iqbal, B. Menaa, A. Razzaq, G. Thiripuranathar, N.F. Rana, F. Menaa, Bioengineering **7**, 1 (2020)
26. M.T. Tran, L.P. Nguyen, D.T. Nguyen, T. Le Cam-Huong, C.H. Dang, T.T.K. Chi, T.D. Nguyen, Res. Chem. Intermed. **47**, 4613 (2021)
27. S. Ninganagouda, V. Rathod, D. Singh, J. Hiremath, A.K. Singh, J. Mathew, M. Ul-Haq, Biomed. Res. Int. **2014**, 1 (2014)
28. J. Saxena, P.K. Sharma, M.M. Sharma, A. Singh, SpringerPlus **5**, 1 (2016)
29. H. Liu, H. Zhang, J. Wang, J. Wei, Arab. J. Chem. **13**, 1011 (2020)
30. M. Tesfaye, Y. Gonfa, G. Tadesse, T. Temesgen, S. Periyasamy, Heliyon **9**, e17356 (2023)

31. M. Riaz, U. Sharafat, N. Zahid, M. Ismail, J. Park, B. Ahmad, N. Rashid, M. Fahim, M. Imran, A. Tabassum, ACS Omega **7**, 14723 (2022)
32. J.U. Chandirika, S.T. Selvi, G. Annadurai, J. Innov. Pharm. Biol. Sci. **5**, 38 (2018)
33. A.P. de Aragao, T.M. de Oliveira, P.V. Quelemes, M.L.G. Perfeito, M.C. Araujo, J.D.A.S. Santiago, V.S. Cardoso, P. Quaresma, J.R. de Almeida Leite, D.A. da Silva, Arab. J. Chem **12**, 4182 (2019)
34. Y. Wang, X. Dong, L. Zhao, Y. Xue, X. Zhao, Q. Li, Y. Xia, Nanomaterials **10**, 83 (2020)
35. Z. Gün Gök, M. Karayel, M. Yiğitoğlu, Res. Chem. Intermed **47**, 1843 (2021)
36. R.F. Elsupikhe, K. Shameli, M.B. Ahmad, Res. Chem. Intermed. **41**, 8515 (2015)
37. V. Soshnikova, Y.J. Kim, P. Singh, Y. Huo, J. Markus, S. Ahn, V. Castro-Aceituno, J. Kang, M. Chokkalingam, R. Mathiyalagan, D.C. Yang, Artif. Cells Nanomed. Biotechnol. **46**, 108 (2018)
38. A. Rautela, J. Rani, M. Debnath, J. Anal. Sci. Technol. **10**, 1 (2019)
39. H.M.M. Ibrahim, J. Radiat. Res. Appl. Sci. **8**, 265 (2015)
40. V. Uma Maheshwari Nallal, K. Prabha, I. VethaPotheher, B. Ravindran, A. Baazeem, S.W. Chang, G.A. Otunola, M. Razia, Saudi J. Biol. Sci. **28**, 3660 (2021)
41. L. Sun, Y. Song, L. Wang, C. Guo, Y. Sun, Z. Li, Z. Liu, J. Phys. Chem. **112**, 1415 (2008)
42. Hemlata, P.R. Meena, A.P. Singh, K.K. Tejavath, ACS Omega **5**, 5520 (2020)
43. D. Sharma, S. Kanchi, K. Bisetty, Arab. J. Chem. **12**, 3576 (2019)
44. S. Suba, S. Vijayakumar, M. Nilavukkarasi, E. Vidhya, V.N. Punitha, Environ. Chem. Ecotoxicol. **4**, 13 (2022)
45. L. Wang, C. Hu, L. Shao, Int. J. Nanomed. **12**, 1227 (2017)
46. T.C. Dakal, A. Kumar, R.S. Majumdar, V. Yadav, Front. Microbiol. **7**, 1 (2016)
47. V. Lavakumar, K. Masilamani, V. Ravichandiran, N. Venkateshan, D.V.R. Saigopal, C.K. Ashok Kumar, C. Sowmya, Chem. Cent. J. **9**, 1 (2015)
48. A.S. Joshi, P. Singh, I. Mijakovic, Int. J. Mol. Sci. **21**, 1 (2020)
49. A. Salleh, R. Naomi, N.D. Utami, A.W. Mohammad, E. Mahmoudi, N. Mustafa, M.B. Fauzi, Nanomaterials **10**, 1 (2020)
50. M.A. Huq, Int. J. Mol. Sci. **21**, 1510 (2020)

Authors and Affiliations

Syafiqah Syazwani Jaffar[1] · Suryani Saallah[1] · Mailin Misson[1] · Shafiquzzaman Siddique[1] · Jumardi Roslan[2] · Wuled Lenggoro[3]

✉ Suryani Saallah
suryani@ums.edu.my

[1] Biotechnology Research Institute, Universiti Malaysia Sabah, Jalan UMS, 88400 Kota Kinabalu, Sabah, Malaysia

[2] Faculty of Food Science and Nutrition, Universiti Malaysia Sabah, Jalan UMS, 88400 Kota Kinabalu, Sabah, Malaysia

[3] Institute of Engineering, Tokyo University of Agriculture and Technology, 2-24-16 Nakacho, Tokyo 184-8588, Japan